

# Electronic structure of the layer compounds GaSe and InSe in a tight-binding approach

M. O. D. Camara and A. Mauger

*Laboratoire des Milieux Désordonnés et Hétérogènes, case 86, 4 place Jussieu, 75251 Paris Cedex 05, France*

I. Devos

*Institut d'électronique et microélectronique du Nord, Département Institut Supérieur d'Electronique du Nord, Avenue Poincaré, 59652 Villeneuve d'Ascq Cedex, France*

(Received 13 July 2001; revised manuscript received 5 November 2001; published 12 March 2002)

The three-dimensional band structure of the III-VI layer compounds GaSe and InSe has been investigated in the tight-binding approach. The pseudo-Hamiltonian matrix elements in the  $sp^3s^*$  basis are fit in order to reproduce the nonlocal pseudopotential band structure, in the framework of constrained optimization techniques using the conjugate gradient method. The results are in good agreement with the optical and photoemission experimental data. The scaling laws appropriate to the covalent bonding are violated by a fraction of eV only, which suggests that the interlayer interactions are not solely of the van der Waals type.

DOI: 10.1103/PhysRevB.65.125206

PACS number(s): 71.20.-b, 71.15.-m

## I. INTRODUCTION

III-VI semiconductors have been extensively investigated since they are considered as layer compounds. Among them, GaSe, and to less extent InSe, have been considered of a particular interest not only for their intrinsic outstanding properties,<sup>1</sup> but also for their potential applications in memory devices.<sup>2</sup> In the late 1950s, early studies on the nature of the chemical bonding in these compounds<sup>3</sup> together with the fact that they crystallize in layered structure<sup>4</sup> have reinforced the idea that the materials under consideration are two dimensional in nature. In this context, most theoretical investigations of the electronic structure in the 1960s have neglected the interlayer interactions,<sup>5,6</sup> although such interactions may affect optical properties. These calculations, however, failed to reproduce even the single layer electronic structure. Hence the feeling that the tight-binding approach, so successful in three-dimensional (3D) materials, was not justified in these layer compounds. Indeed, in the 1970s, the first computations of the electronic structure taking into account interlayer interactions used the pseudopotential approach.<sup>7,8</sup> One has to wait until the late 1970s to find 3D calculations of the electronic structure of InSe<sup>9,10</sup> and GaSe<sup>10,11</sup> using the tight-binding approach. Yet it is hard to justify the rescaling of the two-center integrals used in these works in order to reproduce the proper energy gap. Actually, a significant improvement of the tight-binding formalism has been achieved with the introduction of the  $s^*$  additional orbital, which aims to mimic the effects of the  $d$ -orbitals neglected in the truncation of the Hamiltonian matrix. But this  $s^*$  orbital which allows the  $sp^3s^*$  models to reproduce the band structure and the energy gaps of the semiconductors has been introduced only in the 1980s.<sup>12</sup> Therefore this approach has not yet been used in III-VI compounds.

The current renewed interest in these compounds comes from the successful attempts to grow these compounds by molecular-beam epitaxy.<sup>13,14</sup> In particular, the epitaxy of GaSe and InSe on silicon opens the use of these materials as buffer layers in electronic devices and motivated the present work. In this paper, we report the theoretical study of the

three-dimensional electronic structure of GaSe and InSe in the framework of the tight-binding approach in the  $sp^3s^*$  model. In prior works,<sup>14-16</sup> including the most recent ones,<sup>17</sup> the III-VI compounds are so far considered as truly layered compounds, i.e., it is commonly accepted that the interaction between the layers is weak and solely due to van der Waals interactions. Only the intralayer interactions are supposed to result from an ionic and covalent bonding. However, the interlayer bonding is not as small as in archetypes of layer materials. For example, the ratio  $C_{33}/C_{11}$  between elastic constants in the directions parallel and perpendicular to the layers in  $\epsilon$ -GaSe is 15 times smaller than in graphite,<sup>18</sup> and only three times larger than in three-dimensional materials. Therefore the bonding between layers, although small, is far from negligible, and an order of magnitude larger than expected from van der Waals interaction only. The interlayer interactions in III-VI compounds should then not reduce to the van der Waals interactions, and include a small ionocovalent component as well. Nevertheless, the anisotropic crystal structure implies that the Hamiltonian matrix elements deviate from the scaling laws empirically established for purely covalent bonding.<sup>19</sup> We have thus modified the tight-binding method accordingly. The Hamiltonian matrix elements have been allowed to deviate from the covalent scaling law, and taken as fitting parameters to reproduce the electron dispersion relations determined by the nonlocal pseudopotential approach in GaSe<sup>7,20</sup> and InSe.<sup>21</sup> We find that this tight-binding calculation reproduces the electron dispersion relations determined by the pseudopotential method, for the valence and the lower conduction states as well. Hamiltonian matrix elements determined in the fitting process using the conjugate gradient method are found to deviate by only a fraction of eV from the covalent scaling law. This is another argument that, besides the van der Waals interaction, the interlayer interactions involve ionocovalent bonding which, although small when compared with the intralayer bonding, is far from negligible. Actually, the use of the tight-binding method to determine the electronic structure has two advantages. First, it makes easier the computation of partial densities of states, allowing for a better under-

standing of the bonding in the bulk materials. Second, it allows for the determination of the electronic structure of heterojunctions. In particular, it is very difficult to determine the band offsets by other methods. We used both these advantages which motivated our work to revisit the nature of the electronic band structure and the chemical bonds in bulk III-VI compounds. The electronic properties of their interface with silicon will be the subject of a forthcoming paper.

This paper is then organized as follows. In the next section, we first recall basic features of the crystal lattice. Sections III and IV are devoted to our tight-binding calculation of the three-dimensional electronic structure of GaSe and InSe. The results are displayed in Sec. V and discussed in Sec. VI, with respect to previous tight-binding and pseudo-potential calculations. They are found to reproduce optical and photoemission experimental data. An interesting insight in the nature of the bonds in these compounds is inferred from our model.

## II. CHEMICAL BONDING OF III-VI COMPOUNDS

One layer of GaSe (or InSe) is made of the piling of four atomic planes, two planes of the metal  $M = \text{Ga, In}$  being sandwiched between Se atomic planes. The two dimensional lattice of the atomic planes is hexagonal. This piling is illustrated in Fig. 1, in which the four atomic planes labeled Se1-M1-M2-Se2 constitute one layer. Each atom in the M1 (M2) plane has three Se nearest neighbors (NN) in the Se1 (Se2) atomic plane, respectively (bond labeled 1 in Fig. 1), and one NN metal atom in the M2 (M1) plane. Because of this M-M bond (labeled 2 in Fig. 1), the two M1 and Se1 planes (or mirror M2, Se2 planes) do not merge into one GaSe plane. As a consequence, the Se1-Se2 distance is much larger than the M1-M2 one, and there is a dissimilarity in the local environment between M and Se atoms: each Se atom, say in the Se1 plane, has three M1 NN atoms (bond 1), but no NN Se atom. The nearest Se atom in the Se2 plane which would be the geometric analog of the bond 2 is at a distance which places this Se atom as the fourth nearest neighbor only. The corresponding bonding is negligible. On another hand, we must take into account nearest M-M and Se-Se interactions inside the atomic planes, both labeled 3 and 4, respectively, in Fig. 1. Nevertheless, these considerations show that the nearest M-M bond 2 plays a central role in the chemical bonding and the geometry of the layers. Actually, it determines the optical properties of these materials.<sup>22,23</sup>

The three-dimensional lattices are built by stacking layers. There are, however, different ways of stacking the layers in a compact manner, which correspond to different polytypes. The only type in which GaS is reported to crystallize is the  $\beta$ -type lattice, but GaSe and InSe usually crystallize in the  $\epsilon$ -GaSe,<sup>4</sup> and  $\gamma$ -InSe (Refs. 4, 24, and 25) phase. The  $\beta$ -type corresponds to the staking of adjacent layers illustrated in Fig. 1. The interlayer interaction is dominated by the Se-Se bond (labeled 5 in Fig. 1). The M-Se interlayer bonding is much weaker, not only because the M-Se distance is larger, but also because the M-Se interaction is screened by the

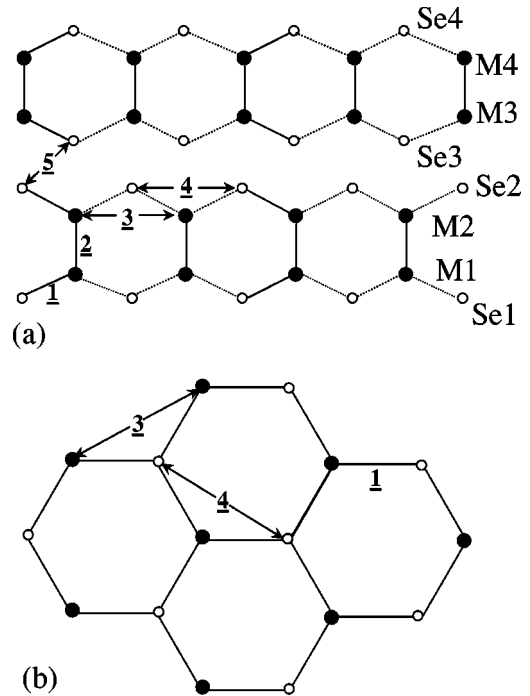


FIG. 1. View of the crystal lattice of  $\beta$ -GaSe and  $\beta$ -InSe (a).  $M$  refers to the metal atom (either Ga or In).  $M1$ ,  $Se1$  refer to the first plane of metal and chalcogen atoms, respectively, building the first half layer. The second half layer is constituted by  $M2$  and  $Se2$  atomic planes. The stacking of the second layer  $Se3$ - $M3$ - $M4$ - $Se4$  has been drawn for the  $\beta$  polytype. The bonds labeled 1–5 correspond to the bonds taken into account in the tight-binding pseudo-Hamiltonian. The  $M$ - $M$  bond 2 between the two half layers connects two metal atoms projected on the same site in the vertical projection (b) in the layer plane. On another hand the interlayer interaction 5 makes the lattice three dimensional.

Se-Se interactions. In this work, only the interactions mentioned above (1–5) are taken into account. This approximation amounts to neglect the differences between polytypes. Band calculations performed in  $\epsilon$ ,  $\beta$ , and  $\gamma$  polytypes corroborate that the energy differences of the electron states throughout the Brillouin zone are small (the order of 0.1 eV).<sup>11</sup> On an experimental point of view, such differences can be estimated from optical studies in  $\text{GaS}_x\text{Se}_{1-x}$ , because, for suitable values of  $x$  in the intermediate region of composition  $0.1 < x < 0.6$ , all three types of stacking occur.<sup>26</sup> Absorption edge measurements have evidenced a difference of energy gap as small as 50 meV between  $\epsilon$ ,  $\beta$ , and  $\gamma$  polytypes.<sup>27</sup> These prior works then show that the differences in the electronic structure between different polytypes are negligible, and justify that we take interactions of the 1–5 kind only. It also means that we have the choice of the polytype to perform our calculations. We only consider the  $\beta$ -type lattice, which has the highest symmetry ( $D_{6h}^4$ ), and contains the smallest number of molecules (eight) in the unit cell. This is also the reason why most of the prior calculations have been performed in this structure, which will make easier the comparison between our results and prior works. The position of the atoms inside the unit cell in this  $\beta$  structure, and the standard notations for the high-symmetry points

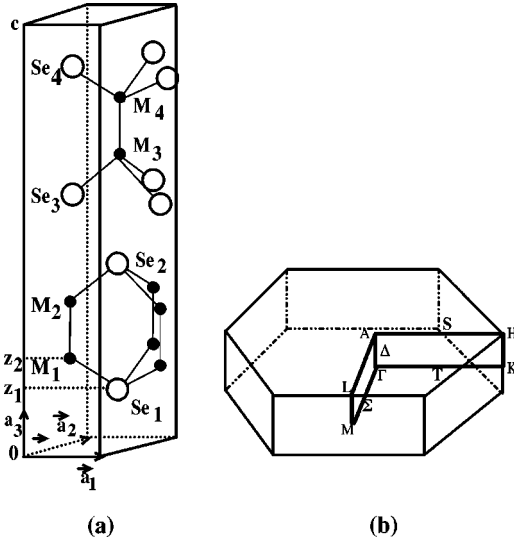


FIG. 2. Unit cell of III-VI compounds in the  $\beta$  polytype (left-hand side). The notation is the same as in Fig. 1. The basis of the lattice is made of the eight atoms labeled  $M1-M4$  and  $Se1-Se4$ . The other atoms are actually outside the unit cell. It implies that some nearest-neighbor interactions connect atoms in different unit cells  $j \neq j'$  in Eq. (3). On the right-hand side of the figure, the corresponding hexagonal Brillouin zone is shown. The high-symmetry points are also indicated, and delimit the irreducible part (heavy contour).

of the corresponding Brillouin zone are illustrated in Fig. 2. The atomic positions of the eight atoms in the hexagonal lattice cell, the fundamental lattice vectors, and the lattice parameters in the  $\beta$  polytype have been reported by Doni *et al.*,<sup>10</sup> after prior works of Kuhn *et al.*<sup>28</sup> for GaSe and Lifkorman *et al.*<sup>29</sup> for InSe. They are reported in Table I, in terms of the parameters  $z_1$  and  $z_2$  defined in Fig. 1 as the smallest distances of the Se and metal atoms from the basic plane.

### III. TIGHT-BINDING CALCULATION OF BAND STRUCTURES OF GaSe AND InSe

The tight-binding Hamiltonian is built in the basis of Bloch states:

TABLE I. Fundamental vectors and positions of the Se and metal (Ga or In) atoms according to their labels in Fig. 1. The numerical data for the lattice parameters are from Refs. 28 and 29 for GaSe and InSe, respectively.

		Basis vectors		
		$\vec{a}_1 = a(\frac{1}{2}, \frac{\sqrt{3}}{2}, 0)$	$\vec{a}_2 = a(-\frac{1}{2}, \frac{\sqrt{3}}{2}, 0)$	$\vec{a}_3 = c(0, 0, 1)$
Positions of Se atoms		Positions of metal atoms		
$Se_1$	$\frac{2}{3}(\vec{a}_1 + \vec{a}_2) + z_1 \vec{a}_3$	$M_1$	$\frac{1}{3}(\vec{a}_1 + \vec{a}_2) + z_2 \vec{a}_3$	
$Se_2$	$\frac{2}{3}(\vec{a}_1 + \vec{a}_2) + (\frac{1}{2} - z_1) \vec{a}_3$	$M_2$	$\frac{1}{3}(\vec{a}_1 + \vec{a}_2) + (\frac{1}{2} - z_2) \vec{a}_3$	
$Se_3$	$\frac{1}{3}(\vec{a}_1 + \vec{a}_2) + (\frac{1}{2} + z_1) \vec{a}_3$	$M_3$	$\frac{2}{3}(\vec{a}_1 + \vec{a}_2) + (\frac{1}{2} + z_2) \vec{a}_3$	
$Se_4$	$\frac{1}{3}(\vec{a}_1 + \vec{a}_2) + (1 - z_1) \vec{a}_3$	$M_4$	$\frac{2}{3}(\vec{a}_1 + \vec{a}_2) + (1 - z_2) \vec{a}_3$	
GaSe	$a = 3.755 \text{ \AA}$	$c = 15.94 \text{ \AA}$	$z_1 = 0.100 \text{ \AA}$	$z_2 = 0.173 \text{ \AA}$
InSe	$a = 4.00 \text{ \AA}$	$c = 16.88 \text{ \AA}$	$z_1 = 0.091 \text{ \AA}$	$z_2 = 0.167 \text{ \AA}$

$$\Psi_{m,\vec{k}}^l(\vec{r}) = N^{-1/2} \sum_j \exp^{i\vec{k} \cdot (\vec{r}_l + \vec{R}_j)} \psi_{jm}^l(\vec{r} - \vec{r}_l - \vec{R}_j). \quad (1)$$

The summation runs over the lattice vectors  $\vec{R}_j$ . The index  $l$  distinguishes between the eight atoms inside one unit cell. The atom  $l$  is positioned at  $r_l$  inside the unit cell.  $m$  labels the orbital type and runs over  $s, p_x, p_y, p_z, s^*$ . To be more specific, the quantum number  $m$  runs over the  $s^*$ ,  $4s$ , and  $4p$  states of Se, and either the  $s^*$ ,  $4s$ ,  $4p$  states of Ga, or the  $s^*$ ,  $5s$ ,  $5p$  states of In.  $\psi_{jm}^l(\vec{r} - \vec{r}_l - \vec{R}_j)$  is the Löwdin  $m$  orbital centered on atomic site  $r_l$  inside the unit cell  $j$ . It is the symmetrically orthogonalized atomic orbital defined by

$$\psi_{jm}^l(\vec{r} - \vec{R}_j) = \sum_{j'm'l'} S^{-1/2}(jml; j'm'l') \phi_{j'm'}^{l'}(\vec{r} - \vec{r}_{l'} - \vec{R}_j), \quad (2)$$

where  $\phi_{j'm'}^{l'}$  is the  $m'$  atomic orbital on atomic site  $l'$  of the unit cell  $j'$ .  $S^{-1/2}(jml; j'm'l')$  is the element between  $\phi_{jm}^l$  and  $\phi_{j'm'}^{l'}$  of the  $S^{-1/2}$  matrix, as defined from the overlap matrix  $S$  between the atomic orbitals. By using Löwdin orbitals instead of atomic orbitals, we obtain a secular equation  $H - \epsilon I = 0$  instead of the one with troublesome overlaps  $H - \epsilon S = 0$  considered in prior tight-binding calculations in GaSe and InSe.<sup>10,11</sup> In the  $\beta$  polytype, the unit cell displayed in Fig. 2 includes eight atoms (four anions and four cations). Since there are five orbitals in the  $sp^3s^*$  basis, the Hilbert space is truncated to a set of  $8 \times 5 = 40$  basis functions. Before introduction of the spin-orbit interaction, we have thus a 40-band model. Since there are  $3 + 6 = 9$  valence electrons per cation-anion pair, or 36 valence electrons per unit cell, the solution of the eigenproblem for the Hamiltonian in this model gives 18 twofold spin degenerate valence bands and 22 conduction bands when the spin-orbit interaction is neglected, twice more when the spin degeneracy is lifted by the spin-orbit interaction. The next step is the calculation of the Hamiltonian matrix elements. In the basis set defined in Eq. (1), they can be written at any given  $\vec{k}$  vector of the Brillouin zone, under the form

$$H_{m_l, m'_l} = \sum_{j'} e^{i\vec{k} \cdot (\vec{r}_{l'} + \vec{R}_{j'} - \vec{r}_l - \vec{R}_j)} \langle \psi_{j_m}^l | H | \psi_{j'_m}^{l'} \rangle. \quad (3)$$

The number of independent matrix elements  $\langle \psi_{j_m}^l | H | \psi_{j'_m}^{l'} \rangle$  is limited by symmetry considerations. Let  $V$  be the generic name for these matrix elements. Although there are five independent values for the quantum numbers  $m, m'$ , the  $s$  and  $p$  symmetries of the orbitals imply that the set  $(m, m')$  gives rise to seven matrix elements noted  $V_{\alpha\beta\gamma}$  in conventional notations of Slater:<sup>30</sup>  $V_{ss\sigma}, V_{sp\sigma}, V_{pp\sigma}, V_{pp\pi}, V_{s^*s^*}, V_{ss^*\sigma}, V_{s^*p\sigma}$ . On another hand, the number of bonds  $(j_l, j'_l)$  between atomic sites inside the unit cell is reduced by the truncation of the interaction to nearest (metal and chalcogen) sites only. For a low-symmetry polytype, this truncation reduces the number of independent bonds to 16. The choice of the  $\beta$  polytype with the highest symmetry reduces the number of nonequivalent nearest-neighbor bonds from 16 to 5 only: the interactions labeled (1)–(5) in Fig. 1. In this sequential order, these bonds can be labeled by an additional index  $\delta$  running from 1 to 5. Therefore the  $\langle \psi_{j_m}^l | H | \psi_{j'_m}^{l'} \rangle$  matrix elements can be written  $V_{\alpha\beta\gamma}^\delta$ . The combination of seven values for the set  $(\alpha\beta\gamma)$  and five values for  $\delta$  results in  $7 \times 5 = 35$  independent such parameters. Within this first-neighbor tight-binding theory pioneered by Harrison<sup>31</sup> to describe the valence bands of semiconductors, and extended to the  $sp^3s^*$  model by Vogl *et al.*<sup>12</sup> to describe lower conduction states as well, we have replaced the actual Hamiltonian by a  $40 \times 40$  (or  $80 \times 80$  when spin-orbit interaction is included) pseudo-Hamiltonian matrix involving 35 independent empirical parameters. The basic idea of the tight-binding theory is to minimize the number of such parameters. In a tetrahedral environment associated to nearly covalent bonding only, such as the zinc-blende structure, the off-diagonal parameters can be estimated from the scaling law:<sup>19</sup>

$$V_{\alpha\beta\gamma} = \eta_{\alpha\beta\gamma} d^{-2} \exp[-2.5(R/d - 1)], \quad (4)$$

where  $d$  is the nearest-neighbor distance between atoms of the same nature as those under consideration,  $R$  the actual distance between the atoms under consideration. The parameters  $\eta_{\alpha\beta\gamma}$  have been determined by Harrison.<sup>32</sup> However, we cannot expect this scaling law to still apply in III-VI compounds which crystallize in a layered structure with hexagonal symmetry. To determine the 35 parameters  $V_{\alpha\beta\gamma}^\delta$ , we then return to the scheme used successfully by Vogl *et al.*<sup>12</sup> in zinc-blende-type semiconductors, i.e., we concentrate on producing energy bands which mimic the nonlocal pseudopotential bands and reproduce the spectral density of states. Of course in the zinc-blende structure, the number of independent parameters is smaller (16) in the nearest-neighbor tight-binding theory, but raises to a value which compares well with 35 when interactions between next-nearest neighbors are included in the pseudo-Hamiltonian. Yet the attempts to determine the electronic structure in such extended-neighbor tight-binding theory faced with the so many adjustable parameters have been successfully achieved in zinc-blende structure, by employing least-square fits to pseudopotential bands.<sup>33</sup> We have followed this procedure, in

the present work, to determine the parameters  $V_{\alpha\beta\gamma}^\delta$  entering the pseudo-Hamiltonian matrix in our nearest-neighbor tight-binding theory of the III-VI compounds.

#### IV. NUMERICAL PROCEDURE

Actually, the independent parameters in the Hamiltonian are the 35 parameters  $V_{\alpha\beta\gamma}$ , plus the energies  $E_\epsilon$  of the pseudo- $s$ ,  $s^*$ , and  $p$  Löwdin orbitals. There are six such parameters labeled by  $\epsilon$  (three for Se plus three for the metal), which raises the total number of independent parameters to 41. The least-square-fit procedure amounts to find the minimum of the function

$$f(\{V_{\alpha\beta\gamma}^\delta\}, E_\epsilon) = \sum_{k,i} (E_k^i - \tilde{E}_k^i)^2 \quad (5)$$

in the space of parameters  $V_{\alpha\beta\gamma}^\delta, E_\epsilon$ . The summation is over a set  $\{\vec{k}\}$  of points in the hexagonal Brillouin zone, and over the valence and lower conduction bands, indexed by  $i$ .  $\tilde{E}_k^i$  corresponds to the dispersion relation as reported from the nonlocal pseudopotential calculations,<sup>20,21</sup> and  $E_k^i$  is the dispersion relation provided by the solution of the eigenproblem of the pseudo-Hamiltonian for a given set  $V_{\alpha\beta\gamma}^\delta$  of independent parameters.

The next step is the choice of the sampling  $\{\vec{k}\}$  of the hexagonal Brillouin zone, over which runs the summation in Eq. (5). If the number of  $\vec{k}$  vectors is too small, the least-square-fit procedure will converge to a solution which reproduces with a high accuracy the energies  $\tilde{E}_k^i$  at these particular points, but will depart from the dispersion relations deduced from pseudopotentials elsewhere in the Brillouin zone. Attention must then be paid to select a number of  $\vec{k}$  vectors large enough to insure the convergence to a solution which reproduces not only the energies  $\tilde{E}_k^i$  at the selected points, but also the overall dispersion relations of the bands. Such a constraint has been achieved by choosing a set of only four  $k$  vectors, namely  $A, \Gamma, K, M$ , plus the point in the middle of the Brillouin zone along the  $\Gamma$ - $K$  direction where the dispersion is larger.

At last, we are left with the choice of the set of energy bands labeled by  $i$  which is the other index entering the summation in Eq. (5). Neither the pseudopotential approach nor the tight-binding approach are supposed to be relevant to describe highly excited states of the conduction band. Therefore the set  $\{i\}$  has been truncated to include all the valence bands, and only the five lowest twofold spin degenerate dispersion curves for conduction electron states (or the ten lowest conduction states when spin orbit is included).

The least-square-fit procedure in Eq. (5) amounts to the search for a minimum of the function  $f$  in the 41-dimensional space of parameters. The numerical procedure we have used for this purpose is the conjugate gradient method, as typified by the Polak-Ribiere algorithm<sup>34</sup> which insures faster convergence than the Fletcher-Reeves algorithm when, like in Eq. (5), the function  $f$  is not quadratic. When the dimension of the space is so large that the steepest descent method is not reliable, the conjugate gradient method is known to al-

ways insure the convergence towards the actual minimum. The  $E_\epsilon$  energies are close to the atomic values which are chosen as the initial values for these parameters in the minimization process of Eq. (5). The starting values for  $V_{\alpha\beta\gamma}^\delta$  completing the set of coordinates of the initial point  $P_0$  of the 41-dimensional space have been chosen equal to the values deduced from the scaling law in Eq. (4), with the  $\eta_{\alpha\beta\gamma}$  reported by Harrison.<sup>32</sup> In addition, we have perturbed the minimization procedure by choosing different starting points in the vicinity of  $P_0$ , yielding different trajectories to converge towards the minimum of  $f$ , and checked that the routine returns to the same minimum.

As usual in tight-binding calculations, and other problems met in physics involving many fitting parameters, such as Rietveld refinements of neutron or x-ray diffractograms<sup>35</sup> or analysis of extended x-ray-absorption fine structure (EXAFS) spectra for example, we have proceeded by different steps. First the fit of the valence bands is achieved in the  $sp^3$  basis, i.e., all the matrix elements involving  $s^*$  are set equal to zero. In this process, the diagonal matrix elements are adjusted first, by considering the energies of the orbitals as fitting variables allowed to depart from the energies of the  $s$  and  $p$  orbitals of the free atoms, aiming to locate the valence-bands at the appropriate energy in the solid. Second, the off-diagonal elements are determined to reproduce the valence band dispersion relations. At last, the  $s^*$  orbital is introduced, aiming to fit the energy gap and the dispersion relations of the first conduction bands. This step by step procedure takes into account the different impact the various parameters have on the band structure, and insures a faster convergence towards the solution. Moreover, it is also a means of controlling that the routine converges to the solution which is meaningful on physical grounds. This control is reinforced by the constraint that the solution does not depart too much from the point  $P_0$ . In particular, we found that all of the 20 actual  $V_{\alpha\beta\gamma}^\delta$  potentials which fit the dispersion relation curves of the valence bands in GaSe and InSe (i.e., those parameters which do not involve  $s^*$ ) depart from their initial value at  $P_0$  by less than 1 eV. As a result, the deviation  $|E_k^i - \tilde{E}_k^i|$  for any valence band  $i$ , at any point of the Brillouin zone along the  $A-\Gamma-K-M$  directions [not only the four  $\vec{k}$  values over which runs the  $k$  index in Eq. (5)], does not exceed 0.3 eV. For matrix elements involving  $s^*$ , we follow the prior works by setting the matrix elements to zero whenever it can be done, i.e., without violating the quality criterion we have imposed. This criterion is that (i) the departure from  $\tilde{E}_k^i$  pseudopotential dispersion curves still does not exceed 0.3 eV for any valence band  $i$ , at any point of the Brillouin zone along the  $A-\Gamma-K-M$  directions. (ii) The energy gap is in quantitative agreement with both the pseudopotential calculations and the experimental data. In other terms, the introduction of the  $s^*$  orbital is intended to adjust the energy gap, without degrading the overall fit of the valence-band structure.

Like in any tight-binding approach, we concentrate on producing energy bands which not only mimic the nonlocal pseudopotential bands,<sup>36</sup> but also reproduce the spectral den-

sity of states.<sup>12</sup> The expression of the density of states, or the imaginary part of the dielectric constant  $\epsilon''(\omega)$ , takes the form

$$\frac{1}{\Omega} \int \int \int_{BZ} F_k^i \delta(E_k^i - E) d^3k, \quad (6)$$

where  $\Omega$  is the volume of the Brillouin zone. The expression has been written in the form appropriate to the calculation of the density of states. In the case of the dielectric constants,  $E_k^i$  has to be substituted by the energy difference  $\Delta E_k^{ij}$  between two bands  $i$  and  $j$ . In both cases, however,  $E_k^i$  or  $\Delta E_k^{ij}$  has the periodicity of the reciprocal lattice. Such integrals over the Brillouin zone, can be determined by replacing the integral by a discrete summation over the ‘‘special  $\vec{k}$  points,’’<sup>37,38</sup> provided the Dirac functions are smoothed. For this purpose, the Dirac distribution has been replaced by a Gaussian of width  $\sigma=0.2$  eV. This value of  $\sigma$  is large enough to insure that the integrand is smooth so that the special point approximation is valid, and small enough so that the peaks in the density of states are not smeared out in the process. The reflectivity curve has been investigated both experimentally, and theoretically by computing first the imaginary part of  $\epsilon''(\omega)$ , then the real part by Kramers-Kronig transformation.<sup>23</sup> These authors have determined that the use of two special  $\vec{k}$  points was already satisfactory to describe the reflectivity curve in the range of energies (3–6 eV) where it has been investigated. However, we found that more than three special  $\vec{k}$  points had to be used to determine quantitatively the partial or total density of states, and we actually used a set of eight special  $\vec{k}$  points in the hexagonal Brillouin zone generated by the procedure of Chadi and Cohen.<sup>38</sup> Note that the reflectivity curves calculated from the band structure determined in the pseudopotential approach are in good agreement with the experimental data in GaSe and InSe.<sup>7,20,23</sup> Since our tight-binding model is built in such a way that we reproduce the nonlocal pseudopotential dispersion relations, we take for granted the fit of the reflectivity curves, and we shall check the validity of the model by direct comparison between theory and experiments, for the dispersion relations and density of states.

## V. TIGHT-BINDING ELECTRONIC STRUCTURE OF GaSe AND InSe

The matrix elements of the tight-binding nearest-neighbor pseudo-Hamiltonian resulting from the least-square fit to the nonlocal pseudopotential dispersion relations, in the framework of the constrained optimization procedure outlined in the previous section, are displayed in Tables II and III. The diagonal intra-atomic elements, which represent the pseudo-atomic energies of the Löwdin orbitals, are reported in Table II together with the  $s$ - and  $p$ -atomic energies of the free elements, to evidence that the departure from the atomic values is actually small, as it should be. The matrix elements  $V_{\alpha\beta\gamma}^\delta$  fit to the pseudopotential band structure are reported in Table III. To get more insight in the chemical bonding in the materials, we have detailed in Table IV the  $V_{\alpha\beta\gamma}^\delta$  evaluated from

TABLE II. Diagonal matrix elements of the tight-binding nearest-neighbor pseudo-Hamiltonian resulting from the least-square fit of the nonlocal pseudopotential dispersion relations. The  $s$ - and  $p$ -atomic energies of the free elements are also reported in parentheses, for comparison. All the energies are expressed in eV.

	GaSe		InSe	
	Ga	Se	In	Se
$E_s$	-12.63 (-11.55)	-22.60 (-25.78)	-12.97 (-10.14)	-21.73 (-25.78)
$E_p$	-6.44 (-5.67)	-12.30 (-10.96)	-6.73 (-5.37)	-10.82 (-10.96)
$E_s^*$	-2.60	-4.89	-2.34	-4.89

the scaling law [Eq. (4)] in case of nearly covalent bonding with the  $\eta_{\alpha\beta\gamma}$  parameters given in Ref. 32. The difference between our result for  $V_{\alpha\beta\gamma}^\delta$  (Table III) and the corresponding element in Table IV allows us to point out deviations from covalent bonding. This difference is found smaller than 1 eV for any matrix element.

The solution of the eigenproblem for the Hamiltonian defined in Tables II and III is reported in Figs. 3 and 4 for GaSe and InSe, respectively. The top of the valence band has been chosen as the origin of energies. For clarity, the dispersion relations and the corresponding Hamiltonian matrix elements have been reported without including the spin-orbit interaction in the pseudo-Hamiltonian. We have also performed the calculations including the spin-orbit interaction  $H_{so}$ . The coupling constant defined as the intra-atomic matrix element  $\lambda = \langle x\uparrow | H_{so} | z\downarrow \rangle$  for Ga, In, and Se has been taken from Ref. 39. The only sizeable effect of this interaction is the lift of the spin degeneracy of the dispersion relations, mainly at the points of the Brillouin zone where the symmetry is high:  $A, \Gamma, M$ , and along the  $M-\Gamma$  direction where the spin splitting is maximum. Yet this splitting remains smaller than 50 meV even in this direction, for any subband. This is a too small splitting to be detected experimentally, and indeed, no spin-orbit effect has ever been reported in III-VI compounds. As a consequence, the spin-orbit interaction will be neglected in the following.

The letters  $A-E$  in Figs. 3 and 4 also label peaks of the density of valence states illustrated in Fig. 7 for the case of

GaSe. The experimental density of states deduced from the analysis of photoemission data<sup>40</sup> is also reported in Fig. 7 for comparison. The width of the valence band extending from the bottom of the  $E$  subband to the top of the  $A$  subbands is 6.8 and 6.6 eV for GaSe and InSe, respectively, in our model. This is in agreement with the experimental estimation of this bandwidth, 7 eV after Ref. 41 in GaSe, and 6.2 eV in InSe.<sup>42</sup> A similar agreement is found with previous tight-binding calculations according to which the bandwidth is 7.2 eV in GaSe,<sup>10,11</sup> and 5.8 eV in InSe.<sup>10</sup> The tight-binding determination of this bandwidth is then in better agreement with experiments than the pseudopotential calculations which predict a width of 6.2 eV only, in GaSe.<sup>23</sup> In addition, the location of the peaks of density is in quantitative agreement with experiments. The  $F$  peak corresponding to the lowest valence band is found at  $-12.3$  eV below the top of the valence band, which compares well with the experimental value  $-12.8$  eV,<sup>40</sup> at contrast with former tight-binding calculations, which places this  $F$  band at lower energy, namely  $-14$  eV (Ref. 10) and  $-14.3$  eV.<sup>11</sup> The only sizeable difference between experiments and our results in Fig. 7 concerns the relative amplitude of the  $D$  and  $E$  peaks. We find the  $E$  peak smaller than the  $D$  peak, at contrast with earlier photoemission data.<sup>40</sup> However, more recent angle-resolved photoemission experiments in the geometry where the photoelectrons are collected along the  $\Gamma M$  direction<sup>43</sup> give  $D$  and  $E$  peaks with the same energy position, and the same relative amplitude as our theoretical result.

TABLE III. Off-diagonal matrix elements of the tight-binding nearest-neighbor pseudo-Hamiltonian resulting from the least-square fit of the nonlocal pseudopotential dispersion relations. The labeling of the bonds in the first column is defined in Fig. 1. All the energies are expressed in eV.

<b>GaSe</b>	$ss\sigma$	$sp\sigma$	$pp\sigma$	$pp\pi$	$s^*p\sigma$	$s^*s\sigma$	$s^*s^*\sigma$
Ga-Se(1)	-0.988	2.057	2.803	-0.533	0.822	-0.333	2.253
Ga-Ga(2)	-2.241	1.881	2.462	-1.013	0.000	-0.279	-0.240
Ga-Ga(3)	-0.102	0.085	0.774	-0.115	0.561	0.007	0.415
Se-Se(4)	-0.133	0.242	0.330	-0.075	0.488	-0.386	1.110
Se-Se(5)	-0.050	0.051	0.483	-0.149	0.249	-0.010	-0.125
<b>InSe</b>	$ss\sigma$	$sp\sigma$	$pp\sigma$	$pp\pi$	$s^*p\sigma$	$s^*s\sigma$	$s^*s^*\sigma$
In-Se(1)	-1.001	2.105	3.290	-0.421	0.913	0.000	0.000
In-In(2)	-1.701	1.493	2.327	-0.968	1.896	0.000	0.000
In-In(3)	-0.133	0.293	1.119	0.204	0.597	0.000	0.000
Se-Se(4)	0.082	0.233	0.114	-0.109	-0.220	0.000	0.000
Se-Se(5)	-0.055	-0.147	0.582	-0.159	-0.051	0.000	0.000

TABLE IV. Off-diagonal matrix elements of the tight-binding nearest-neighbor pseudo-Hamiltonian, after the scaling law (Ref. 19) [Eq. (4) in the present paper]. These matrix elements, with all the  $ss^*\sigma$  and  $s^*s^*\sigma$  elements set equal to zero, completed by the diagonal elements in parenthesis in Table I, define the Hamiltonian in the standard tight-binding scheme (Ref. 12). The labeling of the bonds in the first column is defined in Fig. 1. All the energies are expressed in eV.

GaSe	$ss\sigma$	$sp\sigma$	$pp\sigma$	$pp\pi$	$s^*p\sigma$
Ga-Se(1)	-1.636	1.761	2.752	-0.781	1.825
Ga-Ga(2)	-1.734	1.866	2.917	-0.828	1.765
Ga-Ga(3)	-0.525	0.565	0.883	-0.251	0.545
Se-Se(4)	-0.136	0.146	0.228	-0.065	0.139
Se-Se(5)	-0.116	0.125	0.195	-0.055	0.122
InSe	$ss\sigma$	$sp\sigma$	$pp\sigma$	$pp\pi$	$s^*p\sigma$
In-Se(1)	-1.429	1.537	2.403	-0.682	1.593
InIn(2)	-1.335	1.436	2.246	-0.637	1.358
InIn(3)	-0.510	0.549	0.859	0.244	0.530
Se-Se(4)	0.092	0.099	0.155	-0.044	0.094
Se-Se(5)	-0.119	0.128	0.200	-0.057	0.125

Some information on the dispersion relations of the valence bands are provided by angle-resolved photoemission experiments for GaSe (Ref. 41) and InSe.<sup>42</sup> To go further in the discussion, attention should be paid to the process itself. In such experiments, a photoelectron has to exit from the

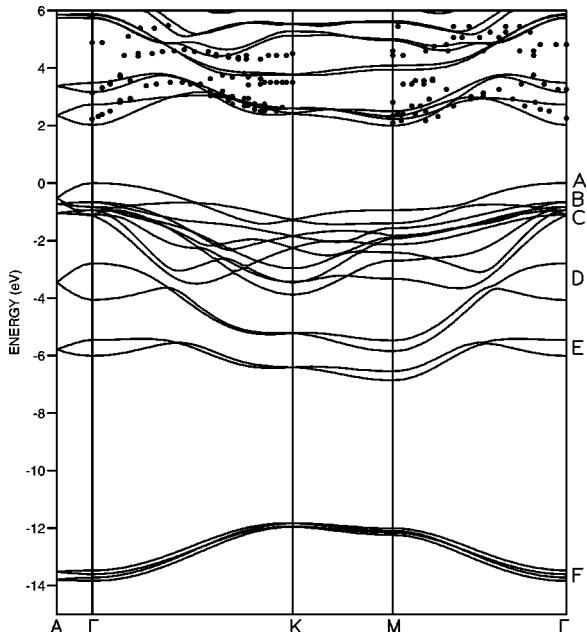


FIG. 3. Band structure of GaSe in our model. The origin of energies is chosen at the top of the valence band. The letters A–F identify the dispersion relation curves responsible for peaks in the density of states, with the same label (see Fig. 7). The result of  $k$ -resolved inverse photoemission spectroscopy experimental data (full dots) relative to conduction bands are also reported, for comparison (Ref. 51).

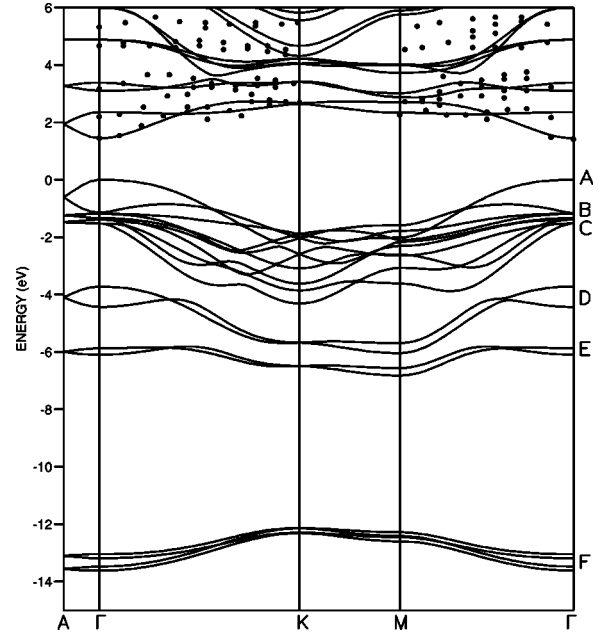


FIG. 4. Band structure of InSe in our model. The origin of energies is chosen at the top of the valence band. The labeling A–F is the same as in Fig. 3. The result of  $k$ -resolved inverse photoemission spectroscopy experimental data (full dots) relative to conduction bands are also reported, for comparison (Ref. 51).

material before being detected. In the process, it crosses the surface, which breaks the translational invariance along the  $z$  axis, and there is no conservation rule for the  $z$  component  $k_z$  of the photoelectron wave vector. Therefore the dispersion relation in angle-resolved photoemission experiments is deduced from an analysis of the spectra in which only the component  $k_{||}$  of the photoelectron is conserved, without taking the  $k_z$  component into account: it is assumed that there is no dispersion of the energy along the  $z$  axis. As stated by the authors themselves, the angle-resolved photoemission experiments then give only access to the 2D dispersion relations of the valence bands.<sup>41,42</sup> To make contact with these experiments, we thus have to mimic also a 2D approximation. To do so, we have considered our Hamiltonian appropriate to bulk GaSe and InSe, as defined by its matrix elements in Tables II and III, in which we set equal to zero all the matrix elements relative to interlayer interactions. The dispersion relations of the valence-band solutions of the eigenproblem for this Hamiltonian are reported in Figs. 5 and 6, together with the angle-resolved photoemission data, for comparison. The overall agreement between our model and the experiments is good. It is, of course, not as good as the agreement which can be reached in three-dimensional band calculations where the fitting parameters are just chosen so that the dispersion relations reproduce these data.<sup>10</sup> However, we find it difficult to justify this procedure, as there is some inconsistency in the fitting of two-dimensional dispersion relations by a three-dimensional Hamiltonian. Even in layered compounds such as GaSe and InSe, the width of the dispersion relations along the  $z$  axis reaches 0.8 eV, which sets the limit in the accuracy of the fitting procedure used in this prior work.<sup>10</sup> Note the agreement between

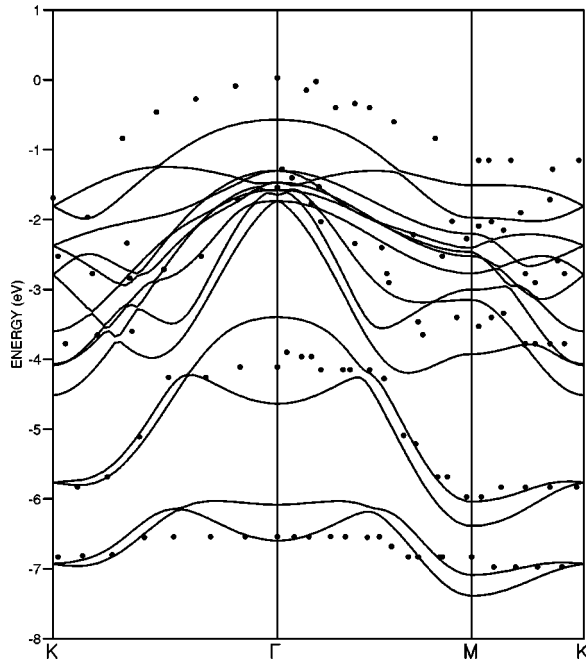


FIG. 5. Comparison between our calculated two-dimensional dispersion relations for the valence bands of GaSe (full curves) and the angle-resolved photoemission experimental data (Ref. 41) (full dots). Note that, due to the two-dimensional nature of both experimental and theoretical results, the dispersion relations do not match the three-dimensional results displayed in Fig. 3.

theory and photoemission experiments in Figs. 5 and 6 is actually better than 0.8 eV for all the bands labeled A–E in Figs. 3 and 4, everywhere in the Brillouin zone.

Most band calculations reproduce more or less the energy gap, since they involve parameters which are adjusted for this purpose. This is also the case in our model: the comparison of the theoretical and experimental energy gaps is a test of efficiency of the addition of the  $s^*$  orbital to the  $sp^3$  basis. Our tight-binding band structure, and the nonlocal pseudopotential band structure we have fit, are calculated with the lattice parameter and interatomic distances set equal to the experimental value measured at room temperature. Therefore the direct and indirect energy gaps in our own calculations must be compared to their experimental value measured at room temperature determined at 300 K. For GaSe, different optical measurements of the gaps have been made<sup>44–47</sup> at different temperatures. All of them are consistent, provided the temperature dependence of the gap is taken into account. As a result, at room temperature, the direct gap in GaSe is 2.03 eV, and the indirect gap is at 1.98 eV. It is commonly accepted that the direct gap is at the center of the Brillouin zone, while the indirect gap is between the top of the valence band at the  $\Gamma$  point, and the bottom of the conduction band at  $M$  point. Our theoretical value is 2.01 and 2.00 eV for the direct and indirect gaps, respectively, in GaSe, in quantitative agreement with experiments. For comparison, too small values, 1.75 and 1.70 eV, are found for the direct and indirect gaps, respectively, in Ref. 10. This is presumably due to the different fitting procedure we have just questioned, giving too much importance to the two-dimensional dispersion re-

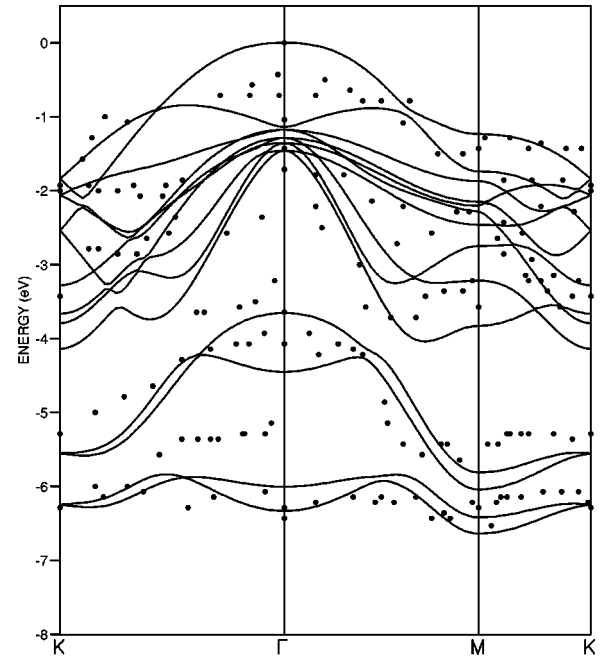


FIG. 6. Comparison between our calculated two-dimensional dispersion relations for the valence bands of InSe (full curves) and the angle-resolved photoemission experimental data (Ref. 42) (full dots). Note that, due to the two-dimensional nature of both experimental and theoretical results, the dispersion relations do not match the three-dimensional results displayed in Fig. 4.

lations of the valence bands. Another tight-binding calculation gives larger values, namely 2.18 and 2.13 eV for the direct and indirect gaps in GaSe.<sup>11</sup> Pseudopotential calculations reproduce quantitatively the direct gap.<sup>23,20</sup> However, if there is also a quantitative agreement with experiments and our own result for the indirect gap in Ref. 20, a smaller value 1.8 eV is found in Ref. 23. For InSe, we find the direct energy gap is 1.44 eV, and the indirect gap is 2.33 eV, with the second minimum of the conduction band still located at the  $M$  point of the Brillouin zone, just like in  $\beta$ -GaSe. On an experimental point of view, InSe has been much less investigated than GaSe.<sup>48</sup> The direct gap at room temperature deduced from absorption measurements is 1.29 eV,<sup>49</sup> in reasonable agreement with our theoretical result 1.44 eV. However, the indirect gap in the same work is reported at 1.19 eV. Another analysis of optical properties of InSe has led Balkanski *et al.*<sup>50</sup> to attribute the indirect gap to an energy 1.8 eV, with the secondary minimum for the conduction band at the  $K$  point of the Brillouin zone, rather than the  $M$  point. This is in contradiction with theoretical calculations in the present work, and previous ones as well, which predict a larger indirect gap, with the secondary minimum of the conduction band at the  $M$  point. Recent experimental techniques such as the  $k$ -resolved inverse photoemission spectroscopy (KRIPES) allow for a better determination of the gaps and discriminate between these conflicting results. Such experiments are intended to give the three-dimensional dispersion relation of the conduction bands, while the angle-resolved photoemission experiments give a two-dimensional approach of the valence bands. Most recent KRIPES experiments on

TABLE V. Energies (in eV) of the bottom of the conduction band at the main points of the Brillouin zone ( $\Gamma, K, M$ ) with respect to the absolute maximum of the valence band at the  $\Gamma$  point. The experimental results of  $k$ -resolved inverse photoemission spectroscopy (KRIPES) are from Ref. 51.

	$\Gamma$		$K$		$M$	
	GaSe	InSe	GaSe	InSe	GaSe	InSe
This work	2.01	1.44	2.42	2.65	2.00	2.33
KRIPES	2.22	1.44	2.38	2.69	2.09	2.25

both GaSe and InSe have been reported by Sporken *et al.*<sup>51</sup> In this study, the authors have explored the  $\Gamma K$  and the  $\Gamma M$  directions. The results are displayed in Figs. 3 and 4 for GaSe and InSe, respectively, together with our own results for comparison. The KRIPES energies at the bottom of the conduction band at the  $\Gamma$ ,  $K$ , and  $M$  points of the Brillouin zone are reported in Table V, together with our theoretical result. A global shift in energy of the KRIPES data has been performed, since the origin of energies in the experiments is unknown. This shift has been chosen in order to adjust the bottom of the conduction band to our theoretical estimation of the smallest gap, which is not controversial as there is an overall agreement between experimental and theoretical estimations of this parameter. In InSe, where the gap is direct, this minimum of the conduction band is 1.44 eV above the top of the valence band at the  $\Gamma$  point, while in GaSe where the gap is indirect, it is located at the  $M$  point, 2.0 eV above the top of the valence band. We find that our tight-binding energy position of the conduction bands at the  $K$ ,  $M$ , and  $\Gamma$  points of the Brillouin zone are in agreement (also within 0.1 eV) with the KRIPES results both in GaSe and in InSe. Therefore our tight-binding model reproduces the dispersion relation of the lower conduction band in GaSe and InSe determined by KRIPES experiments. In particular, we conclude that the indirect gap in InSe is between the top of the valence band at the  $\Gamma$  point and the bottom of the conduction band at the  $M$  point, at contrast with few former underestimations of the indirect energy gaps in InSe, which eventually placed the secondary minimum of the conduction band at the  $K$  point.<sup>50</sup> Like in the case of GaSe, we find our results concerning the band gaps for InSe in quantitative agreement with a former pseudopotential calculation,<sup>21</sup> while a former tight-binding calculation<sup>10</sup> is in qualitative disagreement with experiments, as it predicts InSe is an indirect gap, in addition with a  $M$  point of the conduction band only 1.00 eV above the top of the conduction band. To summarize, our theoretical results for the band gaps are thus an improvement with respect to former tight-binding calculations, and the introduction of the  $s^*$  orbital has allowed to reproduce both the direct and the indirect band gaps in GaSe and in InSe as well, like the best pseudopotential calculations.

According to Figs. 3 and 4, the good agreement between the dispersion relations of the conduction bands in our model and the experimental ones is not restricted to the vicinity of the energy gap, and it extends up to 4 eV above the top of the valence bands. To our knowledge, the density of conduction states has not been measured in InSe. In GaSe, however, the

first peaks in the density of conduction states have been found at 2.35 and 3.65 eV above the top of the valence band.<sup>41</sup> In our model, these peaks occur at 2.6 and 4.0 eV, in agreement with these experiments. The third peak is located at 6.4 eV in our model. This is in disagreement with an experimental work<sup>41</sup> and a tight-binding result<sup>54</sup> where the third peak is reported at 4.75 eV, but in agreement with photoemission experiments analysis<sup>55</sup> and another tight-binding result<sup>11</sup> which report the peak at 6.4–6.9 eV, and the pseudopotential results at 5.8 eV (Ref. 8) and 6.4 eV (Ref. 20) as well. Significant disagreement with experiments can be observed for more remote conduction bands, but our tight-binding approach is no longer valid for such high energies.

## VI. DISCUSSION

To get a better understanding of the chemical bonding in these materials we have computed the partial densities of states. They are illustrated for GaSe in Fig. 8. Since the bonding is essentially the same in GaSe and InSe, we have chosen GaSe as an example, and will simply point out small differences between GaSe and InSe. The  $F$  peak of densities of states is clearly identified as the  $s$  band of Se. The  $E$  and  $D$  states are mainly  $s$  states of Ga, hybridized with  $x, y$  states of Se. This hybridization is at contrast with the previous claim that the  $E$  and  $D$  peaks of density of states correspond to Ga-Ga bonding and antibonding states, respectively. Indeed, the states are related to the Ga-Ga intralayer interaction, as the Ga contribution to these states is dominant. Nevertheless, although smaller than in the  $C$  and  $B$  states, the contribution of selenium in the  $D$  and  $E$  bands is non-negligible, which explains their rather large dispersion, and their overlap with the  $C$  and  $B$  states corroborated by photoemission experiments.<sup>52,53</sup> The  $z$  states of Ga and Se do not contribute to the  $E$  states, but their contribution to the  $D$  states explains the larger amplitude of the  $D$  peak of density of states with respect to the  $E$  peak in our calculations, in disagreement with Ref. 40 in Fig. 7, but in agreement with

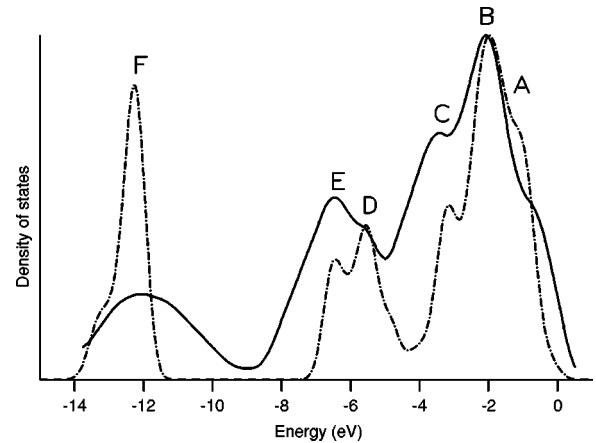


FIG. 7. Comparison between our calculated density of valence states (broken curve) and the result of photoemission experiments analysis (Ref. 40) (full curve) for GaSe. The letters A–F identify peaks associated to the dispersion relation curves with the corresponding label in Fig. 3.

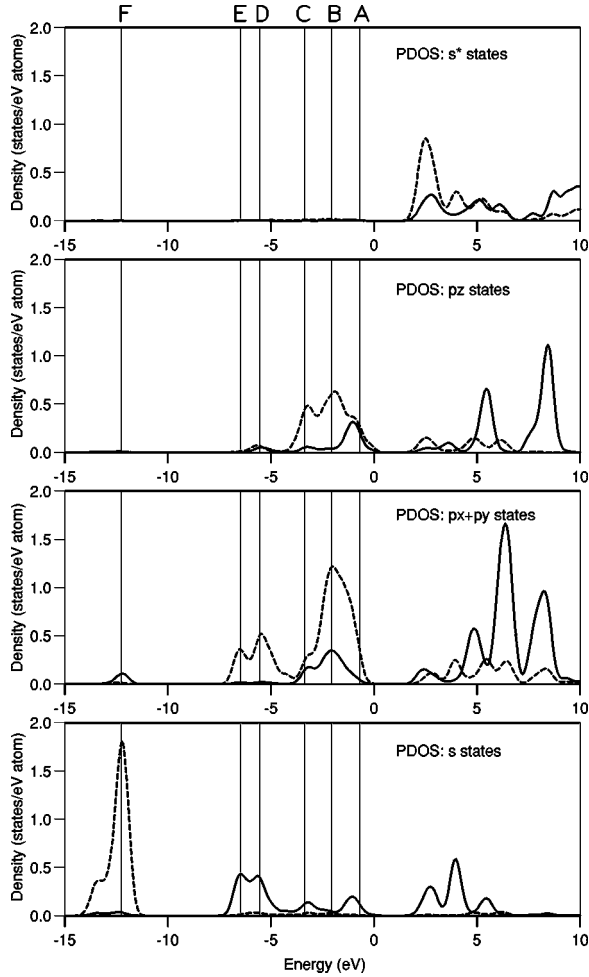


FIG. 8. Partial densities of states in GaSe, on Ga (full curves), and Se (broken curves) atoms. The origin of energies is chosen at the top of the valence band. The vertical lines correspond to the location of the peaks in the state density labeled A–F in Fig. 7.

the more recent angle-resolved photoemission experiments,<sup>43</sup> as already mentioned earlier.

The B and C bands are mainly  $p$  states of selenium, mixed with  $x, y$  states of Ga, so that the corresponding states play a key role in the cohesion of the layers, through the Ga-Se intralayer bonding.

The A-states are of particular importance, since they correspond to the top of the valence band. The calculation of partial densities show a dominant  $p_z$  component of selenium and gallium. This hybridization corresponds to the formation of bonding states due to the  $\sigma$  and  $\pi$  component of the Ga-Se interaction. This is in agreement with former analysis of photoemission experiments with various polarizations of the incident photons.<sup>55</sup> Taking into account that an electron must be in a  $p_z$  valence state to be photoexcited when the polarization of the photon is parallel to the layers, these authors have shown that the states at the top of the valence band are  $p_z$  states of Ga and Se. Figure 8 shows a small  $p_{x,y}$  contribution of Se to the A peak of density of states. However, this contribution comes from states in the A valence band away from the center of the Brillouin zone, i.e., below the top of the valence band. Actually the mixing between  $p_z$

and  $p_{x,y}$  states is forbidden by symmetry at the  $\Gamma$  point of the Brillouin zone.

Although GaSe and InSe valence-band dispersion relations are very similar, some differences can be noticed. First, the splitting between the two D bands at the  $\Gamma$  point is larger in GaSe (1.4 eV) than in InSe (0.85 eV). On one hand, this splitting between these bands vanishes when the interlayer interactions vanish. The dispersion relations are even flat in the  $\Gamma$ -A direction in the 2D model. On another hand, the interlayer distance is smaller and then the interlayer interaction larger in InSe than in GaSe. The larger splitting of these bands in GaSe is thus an evidence that the interlayer interaction is not the only pertinent parameter which determines the splitting energies of the D bands. Actually, we have argued that the D states are sensitive to the Ga-Ga (or In-In) intralayer interaction. Indeed, the larger splitting of the D bands in GaSe is consistent with the fact that the Ga-Ga distance is smaller and the Ga-Ga interaction stronger than the In-In one. In the same way, we have determined that the A states are sensitive to the Ga-Se (In-Se) bond. This is consistent with the larger dispersion of the A band in InSe than in GaSe, as the In-Se distance is smaller than the Ga-Se distance.

The matrix elements  $V_{\alpha\beta\gamma}^\delta$  in Table III, as compared with their initial values predicted for covalent bonding in Table IV, also reveal some aspects of the chemical bonding in the material. The largest matrix elements concerning the coupling is the metal-metal interaction 2 which is then the strongest interaction. We have already argued in Sec. II that this is actually implied by the lattice geometry, and evidenced by optical experiments.<sup>22,23</sup> The parameter  $V_{ss\sigma}$  for this bond is even increased (in absolute value) with respect to the value in Table IV, at the expense of  $V_{pp\sigma}$ . This is due to the fact that the  $p_z$  orbital of the metal is not only involved in the  $M$ - $M$  interaction 2, but also involved in the  $M$ -Se bond 1 inside the semilayers. We also note that the  $V_{sp\pi}$  matrix is non-negligible, and compares well with the initial value in Table IV. This is in essence the reason for the failure of the pioneering works which only took the  $p_z$  orbitals into account.<sup>56</sup> We note that the matrix elements corresponding to this bond 2 are slightly smaller in InSe than in GaSe, which is consistent with the difference in the bonding length. On another hand, the  $V_{ss\sigma}, V_{sp\sigma}, V_{pp\pi}$  elements for the interlayer Se-Se interaction 5 are very small. The interlayer bonding then comes essentially from the  $V_{pp\sigma}$  coupling, which is increased by 0.3 eV in the fitting process. As a result, this interlayer interaction, although much smaller than the intralayer interactions, is not negligible and places these materials in an intermediate position between three-dimensional compounds and truly layered compounds such as graphite or mica. This result is consistent with the ratio  $C_{33}/C_{11}$  of the elastic constants, which characterizes the dimensionality of the material.<sup>57</sup> This is also consistent with most recent first-principles pseudopotential calculations of the structural and dynamical properties, which point out a temperature dependence of the lattice specific heat different from what is expected for truly layered materials.<sup>58</sup>

The above discussion concerning partial densities illustrates the complexity of the mixing between  $s$  and  $p$  states of

the metal and the chalcogen in the eigenwave functions. This is attributable to the low symmetry of the layered compounds, at contrast with the highly symmetric zinc-blende lattice. This is in essence the reason why the spin-orbit interaction has much smaller effects in the IV-VI compounds than in II-V compounds, where the states in the vicinity of the energy gap are pure  $p$  states, although the spin-orbit coupling is roughly the same in GaSe and GaAs. For the same reason, the coupling between  $s^*$  and  $p$  orbitals has small effects on the dispersion relation of the lower conduction band. As a consequence, in GaSe, we found it necessary to adjust the matrix elements  $V_{s^*s\sigma}$  and  $V_{s^*s^*\sigma}$ , while they are set equal to zero in the zinc-blende semiconductors.<sup>12</sup> They could be set equal to zero only in InSe, because this is a direct-gap material, so that the corrections introduced by  $s^*$  are smaller.

## VII. CONCLUSION

We have reported a tight-binding calculation of the IV-VI layered compounds GaSe and InSe, in the framework of the  $sp^3s^*$  model. The parameters of the pseudo-Hamiltonian

have been determined by constrained minimization of the departure from the nonlocal pseudopotential dispersion relations by the conjugate gradient method. The results are in overall agreement with the optical experiments and photoemission experiments, concerning the dispersion relations and the density of states of the valence bands, and the first conduction bands as well. The deviation of the matrix elements with respect to the scaling laws appropriate to covalent bonding in zinc-blende materials is small (a fraction of eV only). In particular, the interaction between the layers is much larger than in graphite, and cannot be reduced to the small van der Waals coupling only, as it has been suggested in the literature.

## ACKNOWLEDGMENTS

M.O.D.C acknowledges financial support from the Ministère de l'Éducation Nationale of Mauritania. The Laboratoire des Milieux Désordonnés et Hétérogènes and Institut d'Électronique et Microélectronique du Nord are associated with Centre National de la Recherche Scientifique.

- <sup>1</sup>A. Segura, J. N. Besson, A. Chevy, and M. S. Martin, *Nuovo Cimento Soc. Ital. Fis.*, B **38**, 345 (1977).
- <sup>2</sup>N. Romeo, *Nuovo Cimento Soc. Ital. Fis.*, B **3**, 103 (1973).
- <sup>3</sup>E. Mooser and W. B. Pearson, *Prog. Semicond.* **5**, 103 (1960).
- <sup>4</sup>W. Schubert, E. Dörre, and M. Kluge, *Z. Metallkd.* **46**, 216 (1955).
- <sup>5</sup>F. Bassani and G. Pastori-Parravicini, *Nuovo Cimento Soc. Ital. Fis.*, B **50**, 95 (1967).
- <sup>6</sup>H. Kamimura, K. Nakao, and Y. Nishina, *Phys. Rev. Lett.* **22**, 1379 (1969).
- <sup>7</sup>A. Bourdon, *J. Phys. (Paris), Colloq.* **C3-261**, (1974).
- <sup>8</sup>M. Schlüter and M. Cohen, *Phys. Rev. B* **14**, 123 (1976).
- <sup>9</sup>Y. Depeursinge, E. Doni, R. Girlanda, A. Baldereschi, and K. Maschke, *Solid State Commun.* **27**, 1449 (1978).
- <sup>10</sup>E. Doni, R. Girlanda, V. Grasso, A. Balzarotti, and M. Piacentini, *Nuovo Cimento Soc. Ital. Fis.*, B **51**, 154 (1979).
- <sup>11</sup>S. Nagel, A. Baldereschi, and K. Maschke, *J. Phys. C* **12**, 1625 (1979).
- <sup>12</sup>P. Vogl, H. P. Hjalmanson, and J. D. Dow, *J. Phys. Chem. Solids* **44**, 365 (1983).
- <sup>13</sup>K. Y. Liu, K. Ueno, Y. Fujikawa, K. Saiki, and A. Koma, *Jpn. J. Appl. Phys., Part 2* **32**, L434 (1993).
- <sup>14</sup>V. Le Thanh, M. Eddrief, C. Sebenne, A. Sacuto, and M. Balkanski, *J. Cryst. Growth* **135**, 1 (1994).
- <sup>15</sup>H. Reqqass, J. P. Lacharme, M. Eddrief, C. A. Sébenne, V. Le Thanh, Y. Zheng, and J. F. Petroff, *Appl. Surf. Sci.* **104-105**, 557 (1996).
- <sup>16</sup>S. El Monkad, M. Eddrief, J. P. Lacharme, K. Amimer, and C. A. Sébenne, *Surf. Sci.* **352-354**, 833 (1996).
- <sup>17</sup>A. Amokrane, F. Proix, S. El Monkad, A. Crincenti, C. Barchesi, M. Eddrief, K. Amimer, and C. A. Sébenne, *J. Phys.: Condens. Matter* **11**, 4303 (1999).
- <sup>18</sup>R. Zallen and M. Slade, *Phys. Rev. B* **9**, 1627 (1974).
- <sup>19</sup>J. O. Fourcade, A. Ibanez, J. C. Jumas, M. Maurin, I. Lefèbre, P. Lippens, M. Lannoo, and G. Allan, *J. Solid State Chem.* **87**, 366 (1990).
- <sup>20</sup>A. Bourdon, Ph.D. thesis, Université de Paris 6, 1983.
- <sup>21</sup>P. Gomes Da Costa, R. G. Dandrea, R. F. Wallis, and M. Balkanski, *Phys. Rev. B* **48**, 14 135 (1993).
- <sup>22</sup>E. Mooser and M. Schlüter, *Nuovo Cimento Soc. Ital. Fis.*, B **18**, 164 (1973).
- <sup>23</sup>M. Schlüter, J. Camassel, S. Kohn, J. P. Voitchovsky, Y. R. Shen, and M. L. Cohen, *Phys. Rev. B* **13**, 3534 (1976).
- <sup>24</sup>J. Rigoult, A. Rimsky, and A. Kuhn, *Acta Crystallogr., Sect. B: Struct. Crystallogr. Cryst. Chem.* **B36**, 916 (1980).
- <sup>25</sup>A. Chevy, A. Kuhn, and M. S. Martin, *Acta Crystallogr., Sect. C: Cryst. Struct. Commun.* **38**, 118 (1977).
- <sup>26</sup>J. L. Brebner, *J. Phys. Chem. Solids* **25**, 1427 (1964).
- <sup>27</sup>E. Aulich, J. L. Brebner, and E. Mooser, *Phys. Status Solidi* **31**, 129 (1969).
- <sup>28</sup>A. Kuhn, A. Chevy, and R. Chevallier, *Phys. Status Solidi A* **31**, 469 (1975).
- <sup>29</sup>A. Lifkorman, D. Carre, J. Etienne, and B. Bachet, *Acta Crystallogr., Sect. B: Struct. Crystallogr. Cryst. Chem.* **31**, 1252 (1975).
- <sup>30</sup>J. C. Slater, *Phys. Rev.* **94**, 1498 (1954).
- <sup>31</sup>W. A. Harrison, *Phys. Rev. B* **8**, 4487 (1973).
- <sup>32</sup>W. A. Harrison, *Phys. Rev. B* **24**, 5835 (1981).
- <sup>33</sup>G. Dresselhaus and A. M. Dresselhaus, *Phys. Rev.* **160**, 6491 (1967); K. C. Pandey and J. C. Phillips, *Phys. Rev. B* **13**, 750 (1976); J. N. Schulman and T. C. Mc Gill, *ibid.* **19**, 6341 (1979).
- <sup>34</sup>See, for example, W. H. Press, S. A. Teukolsky, W. T. Vetterling, and B. P. Flannery, *Numerical Recipes in Fortran, The Art of Scientific Computing* (Cambridge University Press, Cambridge, England), p. 387.
- <sup>35</sup>H. M. Rietveld, *J. Appl. Crystallogr.* **2**, 65 (1969).
- <sup>36</sup>J. R. Chelikowsky and M. L. Cohen, *Phys. Status Solidi B* **68**, 405 (1976).
- <sup>37</sup>A. Baldereschi, *Phys. Rev. B* **7**, 5212 (1973).

- <sup>38</sup>D. J. Chadi and M. L. Cohen, *Phys. Rev. B* **7**, 692 (1973).
- <sup>39</sup>D. J. Chadi, *Phys. Rev. B* **16**, 790 (1977).
- <sup>40</sup>S. P. Kowalczyk, L. Ley, F. R. Mc Feely, and D. A. Shirley, *Solid State Commun.* **17**, 463 (1975).
- <sup>41</sup>P. Thiry, Y. Petroff, R. Pinchaux, C. Guillot, Y. Ballu, J. Lecante, J. Paigné, and F. Lévy, *Solid State Commun.* **22**, 685 (1977).
- <sup>42</sup>P. K. Larsen, S. Chiang, and N. V. Smith, *Phys. Rev. B* **15**, 3200 (1977).
- <sup>43</sup>P. K. Larsen, G. Margaritondo, J. E. Rowe, M. Schlüter, and N. V. Smith, *Phys. Lett.* **58A**, 423 (1976).
- <sup>44</sup>F. Khelladi, Ph.D. thesis, Université de Paris et M. Curie, Paris, 1971.
- <sup>45</sup>A. Balzarotti and M. Piacentini, *Solid State Commun.* **10**, 421 (1972).
- <sup>46</sup>A. Mercier, E. Mooser, and J. P. Voitchovsky, *J. Electrochem.* **7**, 241 (1973).
- <sup>47</sup>M. I. Karaman and V. P. Mushinskii, *Sov. Phys. Semicond.* **9**, 934 (1976).
- <sup>48</sup>A. Bosacchi, B. Bosacchi, and S. Franchi, *Phys. Rev. Lett.* **36**, 1086 (1976).
- <sup>49</sup>M. W. Andriyashik, M. Yu Sakhnovskii, V. B. Timolev, and A. S. Yakimova, *Phys. Status Solidi* **28**, 277 (1968).
- <sup>50</sup>M. Balkanski, C. Julien, and M. Jouanne, *J. Power Sources* **20**, 312 (1987).
- <sup>51</sup>R. Sporcken, R. Hafsi, F. Coletti, J. M. Debever, P. A. Thiry, and A. Chevy, *Phys. Rev. B* **49**, 11 093 (1994).
- <sup>52</sup>F. R. Sheperd and P. M. Williams, *Phys. Rev. B* **12**, 5705 (1975).
- <sup>53</sup>P. M. Williams, *Nuovo Cimento Soc. Ital. Fis., B* **38**, 216 (1977).
- <sup>54</sup>J. Robertson, *J. Phys. C* **12**, 4777 (1979).
- <sup>55</sup>G. Margaritondo, J. E. Rowe, and S. B. Christman, *Phys. Rev. B* **15**, 3844 (1977).
- <sup>56</sup>H. Kanimura and K. Nakao, *J. Phys. Soc. Jpn.* **24**, 1313 (1968).
- <sup>57</sup>A. Polian, Ph.D. thesis, Université de Paris, 1981.
- <sup>58</sup>C. Adler, P. Pavone, and U. Schröder, *Comput. Mater. Sci.* **20**, 371 (2001).